



Effect of pH on produced water treatment using nanofiltration membranes: artificial neural network for performance assessment and steric hindrance pore model for flux variation evaluation

Remya Ravindran Nair^{a,*}, Evgenia Protasova^a, Skule Strand^b, Torleiv Bilstad^a

^aDepartment of Chemistry, Bioscience and Environmental Technology, University of Stavanger, Kjell Arholmsgate 41, 4036 Stavanger, Norway, emails: remya.nair@uis.no (R.R. Nair), evgy.pro@gmail.com (E. Protasova), torleiv.bilstad@uis.no (T. Bilstad)

^bDepartment of Energy and Petroleum Engineering, University of Stavanger, Kjell Arholmsgate 41, 4036 Stavanger, Norway, email: skule.strand@uis.no

Received 30 August 2018; Accepted 13 December 2018

ABSTRACT

Experimental studies have shown that flux and ion rejection by nanofiltration (NF) are strongly influenced by feed pH. The novelty of this research is using the artificial neural network (ANN) in predicting ion rejection based on multiple variable experimental data for feed pH, pressure, and flux. With a number of independent variables affecting ion rejections, ANN is considered suitable compared with Spiegler–Kedem model for predicting the interrelation between variables with non-linear dependencies in a multi-ion environment. However, Spiegler–Kedem and steric hindrance pore models were used for explaining effect of pH on NF flux variations. Experiments were performed to demonstrate reuse of de-oiled produced water (PW) at different pH with salinity similar to seawater as smart water for enhanced oil recovery. Flux was higher at basic pH compared with acidic feed pH and varied due to pH-sensitive dissociable groups, which are protonated or deprotonated with changing pH. An ANN structure was designed that resulted in a close agreement between ANN predictions and experimental data with an agreement of above 95% for all membranes. The results are presented, and interpreted with respect to requirements for smart water, thereby reusing PW, and simultaneously expanding membrane applications in the oil industry.

Keywords: Artificial neural network; Nanofiltration; Spiegler–Kedem; Steric hindrance pore model; Produced water; Smart water

1. Introduction

Water injection is performed during oil production for mostly all oil reservoirs for pressure maintenance and to sustain oil recovery. Amount of produced water (PW) surges as a producing field age and PW volume to be treated is continuously increasing and with high investment for best available technologies.

PW composition is complex and has distinctive characteristics due to organic and inorganic content that differs between reservoirs. The components originate from injected water, formation water, and chemicals including dissolved

and dispersed organic compounds, inorganic compounds including heavy metals, salts, and naturally occurring radioactive materials.

In 2015, only 22% of total PW produced on the Norwegian continental shelf (NCS) were injected into formations while the rest was discharged to sea after treatment. PW discharges were 150 million standard cubic meter (scm) on NCS while oil production totaled 91 million scm in 2015 [1]. Environmental regulations and sustainable development of scarce resources of water are currently moving the focus towards reusing pre-treated PW as injection water.

* Corresponding author.

Enhanced oil recovery (EOR) by smart water has become an accepted technology in the oil industry. Smart water is produced by adjusting the ionic composition of injected water that changes the established equilibrium between crude oil, brine, and pore surface minerals, modifying the wetting properties of reservoirs [2]. In carbonate reservoirs, seawater and modified seawater brines behave as smart water while low salinity brines are more efficient in sandstone reservoirs [2,3].

Smart water for carbonates requires high divalent ion concentrations (SO_4^{2-} , Ca^{2+} , and Mg^{2+}) and low monovalent ion concentrations (Na^+ and Cl^-). For sandstone reservoirs, low salinity water with total dissolved solids (TDS) less than 5,000 ppm and low divalent ion concentrations are preferred [2]. Production of smart water by nanofiltration (NF) membranes using seawater as feed for both reservoirs was discussed in our earlier paper [4]. Permeate is used for smart water production when oil-free PW is treated with NF membranes and is considered as a reuse of PW that simultaneously improves oil recovery and economics [5].

The objective of this research is to focus on PW reuse as smart water for EOR. It has been suggested that NF membranes can treat oil-free diluted PW and reused for EOR in reservoirs [5]. However, pH of PW is one of the main challenges for treatment by membranes. pH of PW differs from 4.3 to 10 depending on reservoirs and chemicals added [6]. TDS of PW vary from hundreds to 250,000 ppm [7].

Experiments were performed for verifying the feasibility of de-oiled PW and seawater co-injection into reservoirs for EOR or for water flooding [8]. The performance of three NF membranes was experimentally determined with respect to flux and ion rejection under a wide range of feed pH and pressure values. The experimental results were later used for predicting ion rejections at given pressure, flux, and pH using artificial neural network (ANN).

A number of mathematical models predict ion transport mechanisms in NF membranes. Prediction of ion rejection was performed by researchers using Spiegler–Kedem model [9–11] to determine the transport parameters reflection coefficient σ and solute permeability P_s [12]. However, these models are mathematically complex and require a detailed knowledge of membrane characterization and performance.

ANN for predicting ion rejection offers a more attractive alternative to Spiegler–Kedem model and has been applied to predict membrane performance and fouling [13,14]. Results showed that proper selection of input variables and number of neurons with a set of training data help to optimize the ANN training process resulting in accurate predictions of membrane performance [15].

This research presents an experimental analysis of membrane performance in terms of flux and rejection using three commercially available NF membranes (NF270, ESNA, and HYDRACoRe50) with seawater with varying pH as feed. Spiegler–Kedem model was used to determine the reflection coefficient and solute permeability of ions. A steric hindrance pore (SHP) model was used to determine the pore size of tested membranes. ANN was used to predict rejections as a function of pressure, pH, and flux for Cl^- , Na^+ , Mg^{2+} , and Ca^{2+} .

2. Theory

Treatment of oilfield PW includes processes such as separators, de-oilers, de-sanders, coagulation, media filters, and membranes. Effective PW treatment generally requires a series of pre-treatment operations to remove contaminants. After appropriate pre-treatment, high TDS can be removed from PW by reverse osmosis (RO). RO membranes have no pores and separation is mainly due to solution-diffusion. However, fouling of RO membranes at high-feed pressure operation is a challenge. NF is an alternative and is a well-established process in separation and purification of solutions. NF membranes have a pore size in the range of 1 nm and operate at feed pressure from 3 to 20 bar and have higher flow rate than RO and are less susceptible to fouling. By implementing NF membrane treatment, the energy consumption will be less than that for RO and increases water recovery.

Performance of NF membranes as a function of pH is analyzed by flux and solute rejection. Membrane characteristics vary with pH [16] and variations are dependent on membrane material, type, and concentration of solute. Solute separation by NF is due to complex mechanisms including Donnan [17] and dielectric effects and steric hindrance. Ion retention is also determined by the distribution of co-ions between the membrane and solution according to Donnan equilibrium for single-salt solutions [18]. However, when pressure is applied across the membrane, Donnan potential repels co-ions and to achieve electroneutrality, counter-ions are also rejected. This is one of the main mechanisms during NF separation [19]. Ion separation also occurs due to sieving (steric) effect based on size differences between ions and membrane pores. Hydrated ions with large size are retained by the membrane while ions with low hydrated radius permeate [19].

2.1. Spiegler–Kedem model

Solute transport through a membrane can be described by irreversible thermodynamics where the membrane is considered as a black box [20]. According to Spiegler and Kedem [20], an expression for relating flux to rejection was developed when high concentration difference occurs between permeate and reject:

$$R_{\text{obs}} = \sigma \frac{(1-F)}{(1-\sigma F)} \quad (1)$$

where

$$F = \exp\left(-\frac{(1-\sigma)}{P_s} J_v\right) \quad (2)$$

where R_{obs} is the observed rejection, J_v is water flux, σ is the reflection coefficient, and P_s is solute permeability.

The parameters σ and P_s were determined by fitting the experimental rejection data R as a function of flux J_v using a best-fit method. The transport parameter σ measures the degree of membrane semi-permeability. A high σ value

($\sigma \approx 1$) indicates that the solute is highly rejected by the membrane [12].

Membrane efficiency is evaluated by measuring flux J_v through the membrane. Flux is defined as permeate flow through a unit area of the membrane surface with units of $L/m^2/h$ and is calculated by Eq. (3) as follows:

$$J_v = \frac{V}{t \times A} \quad (3)$$

where V is the permeate volume, t is the filtration time, and A is the effective membrane area.

Ion rejection R is another parameter used for investigating membrane performance and specifies the concentration of ions in the retentate or percentage of ions rejected by the membrane using Eq. (4).

$$R = 1 - \frac{C_p}{C_f} \quad (4)$$

where C_p and C_f are permeate and feed concentrations, respectively.

2.2. Steric hindrance pore model

According to Nakao and Kimura [21], membrane structural parameters can be estimated using the SHP model. This model was successfully used by many researchers [22,23], to determine the pore size using neutral and charged solutes. The model explains transport of ions through cylindrical pores hindered by frictional forces and the steric effects are considered. According to this model, the membrane parameters σ and P_s are given as:

$$\sigma = 1 - S_F \left\{ 1 + \left(\frac{16}{9} \right) q^2 \right\} \quad (5)$$

$$P_s = D \times S_D \left(\frac{A_k}{\Delta x} \right) \quad (6)$$

where

$$S_D = (1 - q)^2 \quad (7)$$

$$S_F = 2(1 - q)^2 - (1 - q)^4 \quad (8)$$

and

$$q = r_s / r_p \quad (9)$$

D is diffusivity, $A_k/\Delta x$ is the ratio of membrane porosity to membrane thickness, r_s is the Stokes radius of the solute, and r_p is the pore radius. S_D and S_F are the steric hindrance factors for diffusion and convection, respectively. Stokes radius of ions is used to calculate the pore radius and is shown in Table 1.

Table 1
Stokes radii of ions [24]

| Ions | Stokes radius (nm) |
|-------------------------------|--------------------|
| Cl ⁻ | 0.121 |
| Na ⁺ | 0.184 |
| SO ₄ ²⁻ | 0.231 |
| Ca ²⁺ | 0.310 |
| Mg ²⁺ | 0.348 |

2.3. Limitations of membrane process-based models

Proper prediction of NF membrane performance is required for process design and optimization. Ion rejections are mainly predicted by Spiegler–Kedem model and by models based on Nernst–Planck equation. The former is based on a black-box approach that allows the membranes to be characterized based on the transport parameters such as reflection coefficient σ and solute permeability P_s [10,21]. The latter model describes ion transport in terms of effective membrane charge density and ratio of effective membrane thickness to porosity [25]. Both these models were developed from NF membranes physical properties and performance and require a detailed knowledge of the feed conditions and membrane type that may not be readily available.

However, prediction of ion rejection by ANN only requires readily available inputs with a minimum understanding of the overall complexity of the membrane properties. ANN is user-friendly and suitably accurate for industrial design purposes.

2.4. Artificial neural network

ANNs are computational models that act as powerful tools to predict output data in complicated systems with several input parameters with a considerable reduction in time and cost. ANNs are used to process data and provide information using a group of integrated process units called neurons. ANNs are adaptive systems that could change its structure based on the information that flows through the network during the training phase. The multi-layer perceptron artificial neural network includes an input layer, a hidden layer, and an output layer. The number of input layers is three and consists of pH, pressure, and flux. Output values are four and include Cl⁻, Na⁺, Mg²⁺, and Ca²⁺ rejection.

Feedforward back propagation network type is used in this research. In each neuron, the sum of input values is weighted and the sum is transferred through a transfer function. The transfer function calculates the output from an input neuron. The transfer functions mainly used in ANN to solve regression problems are the hyperbolic tangent sigmoid transfer function (tansig), log-sigmoid transfer function (logsig), and the linear transfer function (purelin). The neurons can use any transfer function to create the output. The transfer functions generate outputs for tansig in the range of $-1 \leq f(A_i) \leq +1$, for logsig in the range, $0 \leq f(A_i) \leq 1$ and for linear function from the range $-\infty \leq f(A_i) \leq +\infty$, where A_i is the net input [26]. Different number of hidden layers can be used and the number of neurons in each layer is varied to find the best ANN structure to predict ion rejection.

The ANN inputs present the variables that have an effect on the predicted outputs such as pH, pressure, concentration, and membrane type. All these inputs are related to ion rejection, the ANN output in this research. The structure of the neural network used to predict ion rejection in this research is shown in Fig. 1.

The output layer should have four neurons since the number of outputs is four. The selected training algorithm is Levenberg–Marquardt. There are mainly four steps involved in ANN modeling that include collecting the training data for input and output, selecting the network design, training the network, and network simulation. The most important phase of building the ANN model is network training. During the training phase, the data supplied will be divided into three sections that include the training data, validation data, and test data. The training process minimizes the error related to the deviations of the ANN predictions from the target values and is calculated as mean square error (MSE). The value of MSE is calculated using Eq. (10) [26].

$$MSE = \frac{\sum_{i=1}^n (t_i - a_i)^2}{n} \tag{10}$$

where t_i denotes the i -th target value, a_i is the predicted value, and n is the number of data.

The optimum neural network structure was selected based on the smallest difference between the predicted values and the experimental data or in other words, the neural network with the least MSE and highest R^2 is selected. R^2 is the statistical coefficient of determination and a value higher than 0.95 is considered acceptable.

3. Experimental methods

3.1. NF membranes

Three commercial NF membranes were investigated in this study; Nitto Hydranautics ESNA, HYDRACoRe, and Dow Filmtec NF270. Table 2 summarizes the membrane specifications according to the manufacturers. ESNA and Filmtec NF 270 have a polyamide skin layer on a polysulfone/polyester support layer.

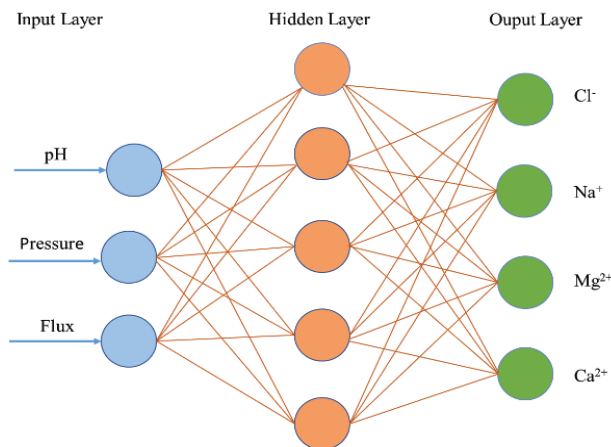


Fig. 1. ANN configuration with five neurons in the hidden layer.

Maximum operating pressure and temperature are 41 bar and 45°C and the pH range is 2–11 for all three membranes.

3.2. Experimental set-up

The experimental set-up consists of membrane modules listed in Table 2, one membrane operated at a time. Membranes were first stabilized by washing with pure water for approximately 4 h at 25°C and 10 bar. Membranes were operated in a cross-flow mode at room temperature with operating pressure of 9–18 bar. Feed seawater was pre-treated through a 20 μm and a 5 μm cartridge filter. The retentate and permeate streams were returned to the feed tank securing identical feed concentrations. Samples from both streams were collected and analyzed. The membrane stabilization time for each experimental run at different feed pH was 25 min at all tested operating pressures. Flux through the membrane was calculated by measuring the permeate flow rate through the active membrane area. The flow rate was measured immediately after 25 min. Three trials were performed for each pH value and the membranes were producing for 3 h for each trial.

3.3. Feed solutions and analytical instruments

Experiments should be performed with de-oiled PW with high TDS for precise calculations. However, for ease of experimental analysis, the experiments were performed by varying the pH in seawater with ionic composition as shown

Table 2
Membrane specifications according to manufactures

| Membrane | Material | Area, m ² | Permeate flow rate, m ³ /d |
|------------------------|-----------------------------|----------------------|---------------------------------------|
| ESNA | Composite polyamide | 2.3 | 4.9 |
| HYDRACoRe ^a | Sulfonated polyethersulfone | 2.3 | 4.2 |
| Filmtec NF270 | Composite polyamide | 2.6 | 3.2 |

^aMolecular weight cut off is 1,000 Dalton according to the manufactures.

Table 3
Compositions of major ions in PW and seawater in mol/L

| | PW ^a | Seawater ^b |
|-------------------------------|-----------------|-----------------------|
| HCO ³⁻ | 0.013 | 0.002 |
| Cl ⁻ | 1.096 | 0.525 |
| SO ₄ ²⁻ | 0.001 | 0.024 |
| Mg ²⁺ | 0.008 | 0.052 |
| Ca ²⁺ | 0.031 | 0.093 |
| Na ⁺ | 1.027 | 0.474 |
| K ⁺ | 0.005 | 0.010 |
| TDS (g/L) | 64.96 | 34.1 |

^aPW composition for Valhall field [8].

^bSeawater composition from ion chromatography (IC) analysis.

in Table 3. It was assumed that the feed seawater used for the experiments can be considered as diluted de-oiled PW with no colloids or scaling ions present. Thus, the effect of colloidal fouling and concentration polarization during membrane performance is not considered. PW composition from the Valhall field in the North Sea [8] is likewise displayed to compare the ionic concentrations between PW and seawater. The ions are identical in both PW and seawater, though the ion concentrations differ. Scaling ions such as barium and strontium were not present in the feed seawater.

Experiments were carried out with pre-filtered seawater at 34,100 ppm TDS and conductivity of 47.3 mS/cm. pH of seawater was adjusted between 2.5 and 10.2 by adding analytical grade HCl and NaOH. 12 feed pH values were used: 2.5, 3, 3.5, 4, 4.5, 5, 6, 7, 8.5, 9.2, 9.7, and 10.2. Experiments were also performed with normal seawater with pH 8. No HCl or NaOH was added at pH 8.

Conductivity, salinity, temperature, and TDS were measured using TDS meter VWR collection CO3100N. pH was measured using VWR Phenomenal pH 1100L. Ion concentrations were measured using IC (Dionex ICS-5000+ DP).

3.4. Membrane cleaning

Suitable membrane cleaning was performed with tap water after each experiment. Flushing was continued until clean water membrane flux returned to its initial flux. pH and conductivity of recirculated water were continuously monitored to confirm that no fouling occurred on the membrane. Chemical cleaning was performed using Aqua Pro Membrane cleaner for removal of metal hydroxides, CaCO₃, and other types of scaling.

4. Results and discussions

4.1. Effect of feed pH on flux or membrane permeability

Membrane performance at various feed pH values was interpreted by analyzing flux through the membrane. Flux as a function of transmembrane pressure for three NF membranes is represented in several figures. Fig. 2 shows the effect of pH on flux with increasing operating pressure for ESNA.

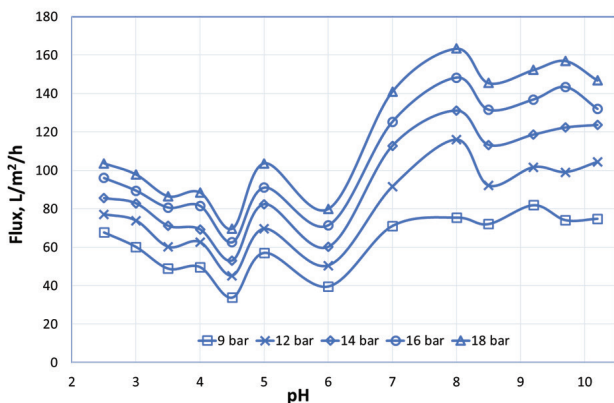


Fig. 2. Flux vs. pressure for ESNA at different pH.

Data presented in the graphs are average values from three trials. Fig. 2 shows that the lowest flux was 34 L/m²/h at pH 4.5 with an operating pressure of 9 bar. Below this pH, flux improved to 68 L/m²/h at 9 bar for pH 2.5. However, when comparing the membrane performance in all tested pH values, pore size shrinkage occurred significantly at acidic conditions. Highest flux was observed when normal seawater permeated through the membrane at pH 8. High flux was observed at basic pH for all pressures. Flux increased linearly at all individual pH with an increase in pressure confirming that no membrane fouling occurred during the experiments.

Fig. 3 displays flux vs. pressure for HYDRACoRe. Low flux was observed at acidic pH and a major change in flux was not observed during the entire tested pH values.

Flux vs. pressure for NF 270 is presented in Fig. 4. Minimum flux was obtained at pH 3. An increase in flux was observed with an increase in feed pH.

Flux for each membrane varies with the type of feed water and increases with increasing pressures. Maximum flux was attained at pH 8 with normal seawater as feed for all three membranes. This confirms that these membranes are designed to produce maximum flux when seawater is used as feed.

Highest flux was 163 L/m²/h observed for ESNA as presented in Fig. 2 and indicates more open pores for ESNA compared with HYDRACoRe and NF 270. ESNA and NF

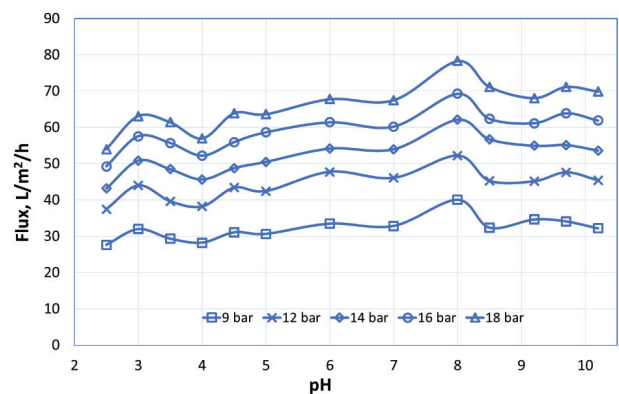


Fig. 3. Flux vs. pressure for HYDRACoRe with varying pH.

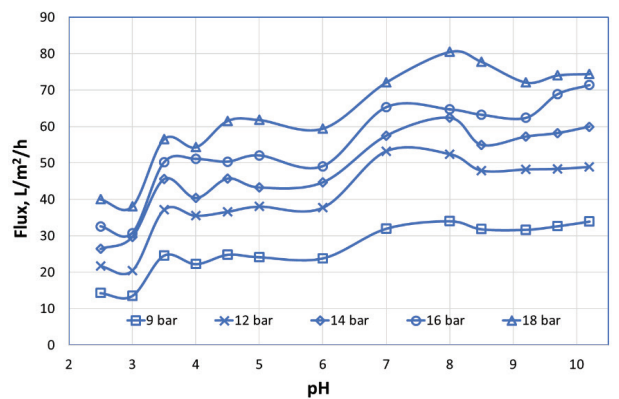


Fig. 4. Flux vs. pressure for NF 270.

270 membranes have a polyamide skin layer. However, they have different degrees of crosslinking that gives rise to different surface properties resulting in different flux and ion rejection pattern as a function of pH. Polyamide NF membranes consist of both carboxyl group ($\equiv\text{COO}^-$) and amino groups ($\equiv\text{NH}_3^+$) and exhibit positive and negative surface charges depending on pH. At acidic conditions, protonation of amine occurs ($\equiv\text{NH}_2 \rightarrow \equiv\text{NH}_3^+$) resulting in increased pore size, thereby increasing flux. This explains a slight peak in flux in an acidic environment at pH 5 in Fig. 2. At high pH, polyamide membrane matrix appears to be more expanded due to deprotonation of carboxyl group ($\equiv\text{COOH} \rightarrow \equiv\text{COO}^-$) resulting in higher flux as in the case of ESNA and NF 270.

HYDRACoRe membranes are made of sulfonated polyethersulfone and have $-\text{SO}_2$ groups in the polymeric sulfone. This is quite stable due to attraction of resonating electrons between adjacent aromatic groups, and the presence of repeating phenylene rings creates steric hindrance to the rotation [27]. Both these characteristics lead to molecular immobility and wide pH tolerance [27]. Fig. 3 also confirms that permeability of HYDRACoRe was quite stable over the tested pH range, except for a slight increase in flux for normal seawater at pH 8.

4.2. Effect of feed pH on ion rejection

The retention of charged ions depends on ion valency, concentration, charge density, surface charge, and chemical nature of the groups present on the membrane surface. Individual ion concentrations at different pressures and pH values in reject and permeate were measured for ESNA, HYDRACoRe, and NF 270. An increase in ion rejection with an increase in pressure was observed in all samples.

4.2.1. Rejection of monovalent ions

Different membranes showed different rejection patterns even with small pH changes, which could be due to different surface characteristics of the three tested membranes. Figs. 5 and 6 display rejection of Cl^- and Na^+ at different feed pH values with increasing pressure for ESNA.

Figs. 5 and 6 present low ion rejections of Na^+ and Cl^- in basic environment. It was observed that when flux increased, ion rejection decreased. In Fig. 2, a flux minimum at pH 4.5

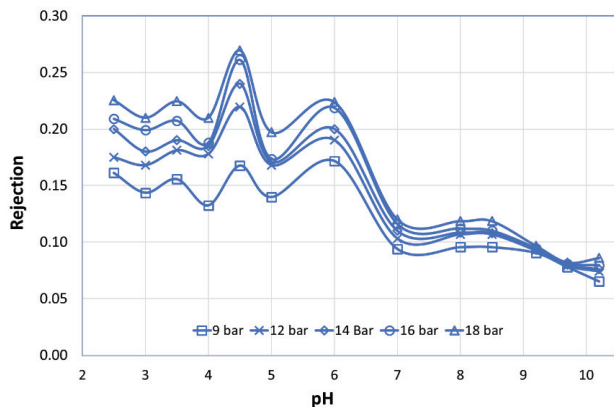


Fig. 5. Cl^- rejection for ESNA.

was observed whereas a peak in rejection at the same pH for Na^+ and Cl^- was observed in Figs. 5 and 6.

Figs. 7 and 8 show the rejection of Cl^- and Na^+ with HYDRACoRe.

Na^+ and Cl^- rejection by HYDRACoRe show similar patterns. A slight decrease in flux with HYDRACoRe was observed at pH 4. However, a peak in monovalent ion rejections was observed at pH 4. The results confirm that Donnan potential influences ion rejection. In Fig. 8, at pH 4, a peak in Na^+ rejection is observed, which could be either due to pore

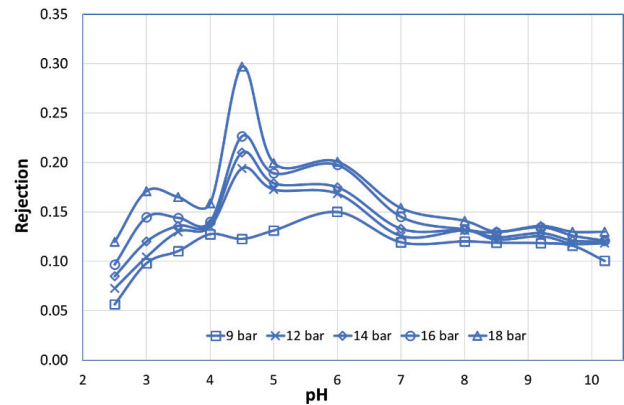


Fig. 6. Na^+ rejection with varying pH for ESNA.

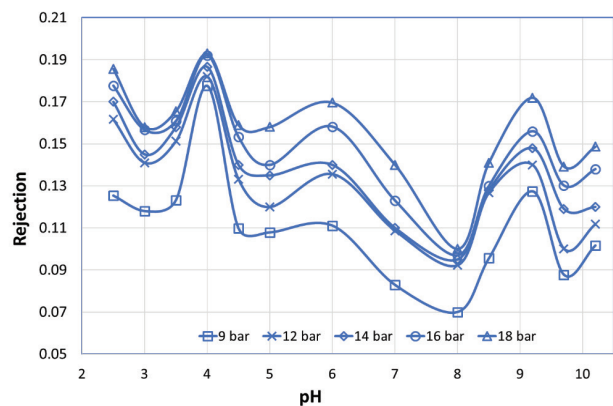


Fig. 7. Cl^- rejection for HYDRACoRe at different feed pH.

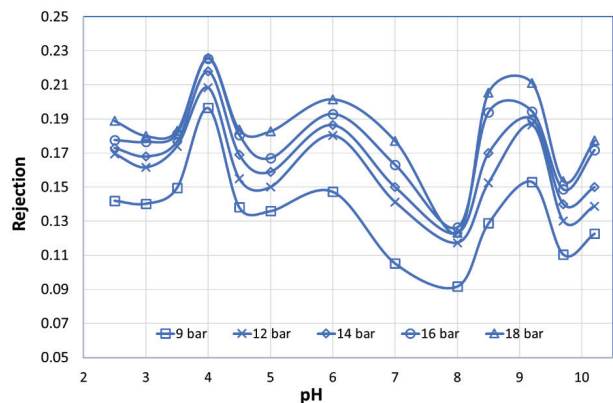


Fig. 8. Na^+ rejection at different feed pH for HYDRACoRe.

size reduction or by repulsion by the positive charge of the membrane. To maintain electroneutrality at pH 4, more Cl⁻ is rejected according to Fig. 7.

Monovalent ion rejection for NF 270 is displayed in Figs. 9 and 10.

It has been confirmed that the isoelectric point for NF 270 is close to pH 5 and salt rejection is minimum at pH 4 [28]. The performed experiments confirmed that Na⁺ and Cl⁻ rejections were low at pH 4.5 for NF 270, close to the isoelectric point.

4.2.2. Rejection of multivalent ions

Figs. 11–13 present the rejection of Mg²⁺ for ESNA, HYDRACoRE and NF 270 membranes.

Highest Mg²⁺ rejection was observed at the lowest tested pH of 2.5 for ESNA. This confirms that the membrane is highly positively charged at acidic conditions and positive charges are reduced with increasing pH values. Rejection of more positively charged Mg²⁺ resulted in permeation of more Na⁺ through the membrane to maintain electroneutrality between two phases of the membrane. This means low rejection of Na⁺ at acidic pH. This explains the comparatively low rejection of Na⁺ at acidic pH. This explains the comparatively low rejection of Na⁺ in Fig. 6.

Figs. 5–13 present ion rejections as a function of pH. SO₄²⁻ is generally not present in PW and is not evaluated in this

research. Results show that ion rejection by HYDRACoRe was less than 35% for all ions confirming that the effect of pH on HYDRACoRe was weak or less at all pH. Highest Mg²⁺ rejection was 98% observed at pH 2.5 for NF 270 and decreased to 56% at pH 10.2. There was only a slight effect of pressure on Mg²⁺ rejections for ESNA and NF 270 since the rejection was almost the same at all operating pressures, whereas a slight increase in Mg²⁺ rejection was observed for HYDRACoRe.

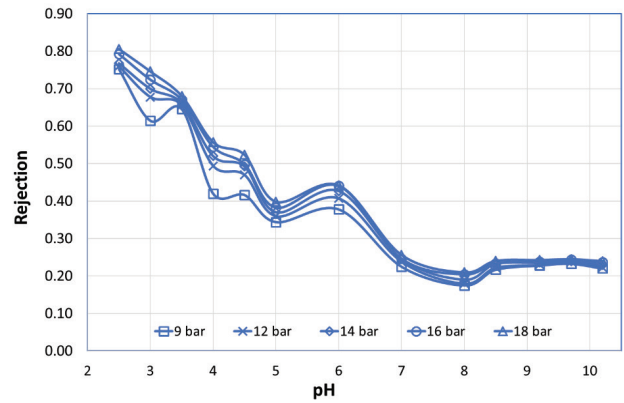


Fig. 11. Mg²⁺ rejection at different feed pH for ESNA.

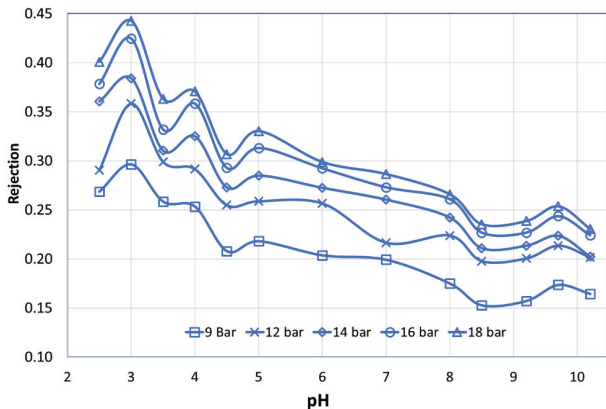


Fig. 9. Cl⁻ rejection at different feed pH for NF 270.

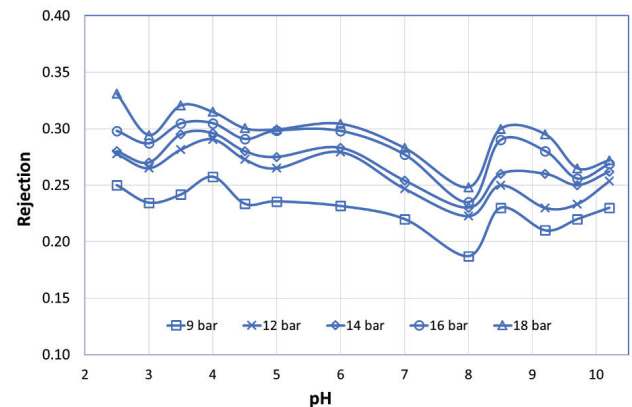


Fig. 12. Mg²⁺ rejection at different feed pH for HYDRACoRe.

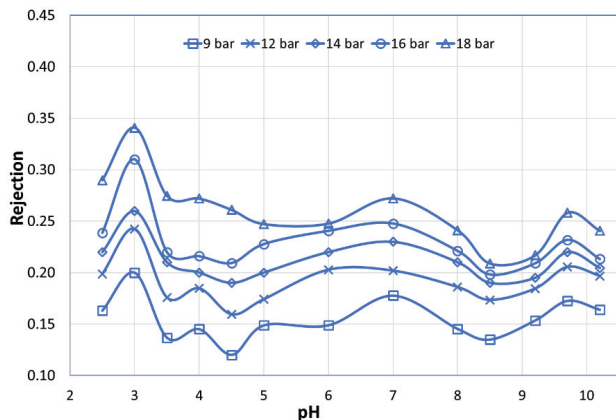


Fig. 10. Na⁺ rejection at different feed pH for NF 270.

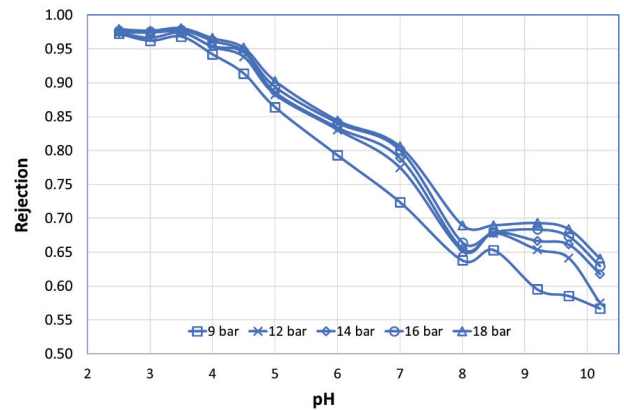


Fig. 13. Mg²⁺ rejection at different feed pH for NF 270.

Fig. 14 shows the rejection of Ca^{2+} for ESNA. The highest Ca^{2+} rejection was observed at low pH. A depression in rejection of Ca^{2+} was observed between pH 5 and 7. The rejection increased at pH 8 (normal seawater) and slightly decreased at $\text{pH} > 8$.

During membrane performance, electrostatic repulsion between the membrane and cations determines ion rejection. When Na^+ , Ca^{2+} , and Mg^{2+} are present in the feed, co-ion rejection competition occurs. Ions with low hydration energy and high mobility are prone to permeate and Na^+ with lowest hydration free energy passes easily through the membrane to balance the charge on both sides. Ca^{2+} has higher hydration energy than Na^+ but lower than Mg^{2+} . Hence, Mg^{2+} will be rejected more than Ca^{2+} as confirmed by Figs. 11 and 14. Hydration free energy of Na^+ , Ca^{2+} , and Mg^{2+} are -365 , $-1,592$, and $-1,922$ kJ/mol, respectively [29]. Similar rejection for Ca^{2+} was observed for HYDRACoRe and NF 270.

Flux and rejections at different pH values may be caused by several mechanisms or combination of mechanisms. These include change in pore size due to change in conformation of the cross-linked polymer structure of the membrane or membrane swelling or shrinkage, difference in osmotic pressure due to addition of HCl or NaOH, changes in electroviscous effect resulting in variation in water permeability, co-ion and counter-ion interactions, Donnan effect, steric or sieving effect, convection, and diffusion.

4.2.3. Pore radius (r_p) calculations using Spiegler–Kedem and SHP models

Characterization of the membrane physicochemical properties such as contact angles, surface morphologies, and membrane surface zeta potentials is generally measured to determine the variations in ion rejections and flux permeation. In this research, membrane performance at different pH values has been analyzed by variations in r_p , calculated using Spiegler–Kedem and SHP models where the single independent variable approach was used.

The membrane transport parameters σ and P_s of each ion was calculated by fitting flux vs. rejection in Eqs. (1) and (2) for the three tested membranes. To explain the difference in pore size, Mg^{2+} is chosen as a reference since the Stokes radius and hydration energy of Mg^{2+} is highest when compared with other ions present in seawater and is a divalent cation and thus will be attracted by the membrane surface. Table 4 shows reflection coefficients and solute permeabilities of Mg^{2+} for the three tested membranes at all observed pH values.

Variations in pore size with pH for all membranes with respect to Mg^{2+} was calculated using SHP model by applying σ and P_s on Eqs. (5)–(9) for the three NF membranes. The resulted r_p for the three membranes are presented in Fig. 15.

The results confirm that when pH is varied, pore size was reduced at acidic pH irrespective of the type of membrane, resulting in decreased flux and increased ion rejection. The original r_p is assumed to be at pH 8 when normal seawater was used as feed since all the three NF membranes are designed to operate with seawater. According to Fig. 15, r_p is lowest at pH 3 and highest at pH 8 for ESNA. When r_p is lowest, flux is at a minimum with increased rejection. However, there is a deviation in flux and rejection behavior for ESNA. Minimum flux was observed at pH 4.5 with a peak in ion rejections at the

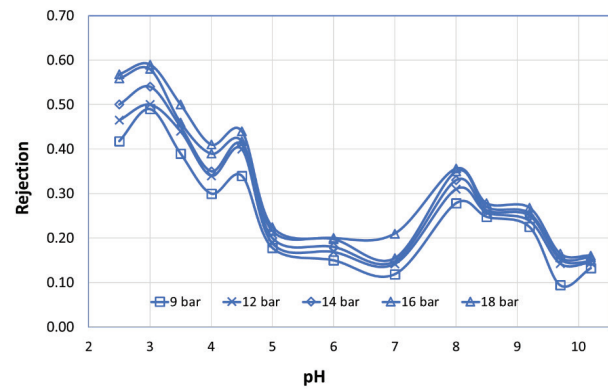


Fig. 14. Ca^{2+} rejection observed for ESNA at different feed pH.

Table 4

Reflection coefficient and solute permeability of Mg^{2+} at varying pH

| pH | ESNA | | FilmTec | | HYDRACoRe | |
|------|----------|------------------------|----------|------------------------|-----------|------------------------|
| | σ | P_s (m/s) | σ | P_s (m/s) | σ | P_s (m/s) |
| 2.5 | 0.84 | 3.578×10^{-6} | 0.98 | 6.258×10^{-8} | 0.37 | 6.202×10^{-6} |
| 3 | 0.85 | 6.629×10^{-6} | 0.98 | 1.181×10^{-7} | 0.32 | 5.921×10^{-6} |
| 3.5 | 0.68 | 2.177×10^{-6} | 0.98 | 1.625×10^{-7} | 0.36 | 6.038×10^{-6} |
| 4 | 0.70 | 9.823×10^{-6} | 0.97 | 2.761×10^{-7} | 0.33 | 4.319×10^{-6} |
| 4.5 | 0.55 | 4.399×10^{-6} | 0.97 | 5.053×10^{-7} | 0.33 | 6.052×10^{-6} |
| 5 | 0.41 | 6.409×10^{-6} | 0.90 | 5.96×10^{-7} | 0.33 | 5.985×10^{-6} |
| 6 | 0.47 | 5.174×10^{-6} | 0.86 | 9.053×10^{-7} | 0.35 | 7.212×10^{-6} |
| 7 | 0.26 | 8.316×10^{-6} | 0.75 | 1.363×10^{-6} | 0.34 | 8.581×10^{-6} |
| 8 | 0.22 | 1.228×10^{-5} | 0.67 | 2.088×10^{-6} | 0.38 | 1.417×10^{-5} |
| 8.5 | 0.24 | 7.763×10^{-6} | 0.69 | 1.449×10^{-6} | 0.29 | 4.383×10^{-6} |
| 9.2 | 0.24 | 7.024×10^{-6} | 0.73 | 3.059×10^{-6} | 0.31 | 5.46×10^{-6} |
| 9.7 | 0.24 | 5.666×10^{-6} | 0.72 | 3.17×10^{-6} | 0.28 | 5.312×10^{-6} |
| 10.2 | 0.24 | 7.407×10^{-6} | 0.65 | 3.038×10^{-6} | 0.28 | 4.455×10^{-6} |

same pH. While comparing the difference in pore sizes with pH, it should be noted that for ESNA and NF 270, the effect of pH was more distinct. For ESNA, r_p decreased from 0.87 to 0.42 nm while for NF 270, r_p decreased from 0.5 to 0.37 nm.

4.3. Effect of PW pH on smart water production

Results obtained confirm that feed water with varying pH can be treated with NF membranes to produce permeate with modified ionic composition. Flux is high when feed pH is basic. Basic pH has the advantage of permeating more divalent ions, which are advantageous for carbonate reservoirs and is confirmed by Figs. 11 and 13. These figures show that when PW feed pH was high, more Mg^{2+} permeated through the membrane. A power consumption analysis on the production of smart water from de-oiled PW for both carbonate and sandstone reservoirs has previously been confirmed [5].

4.4. Modeling ion rejection using ANN

In this research, operating pressure, pH, and flux are considered as variables and used as inputs to the ANN network. The number of neurons in each layer is varied for the

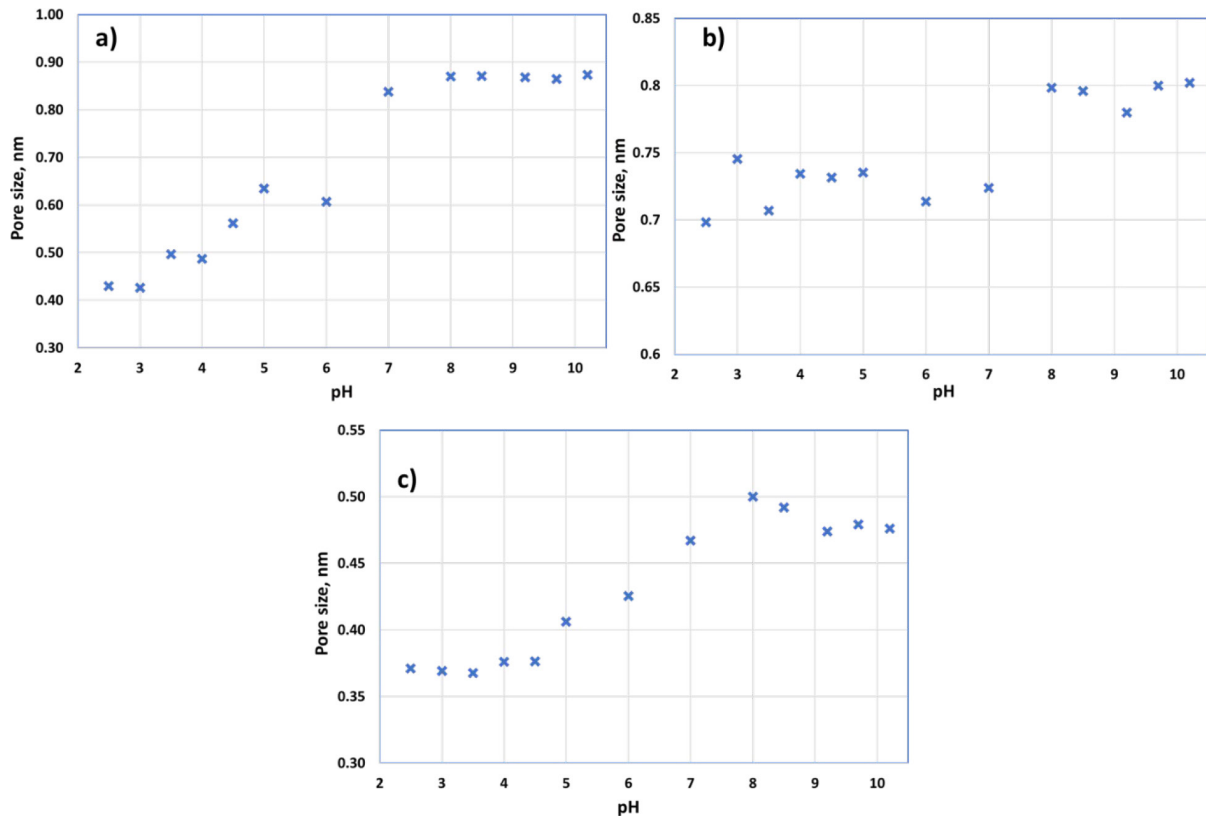


Fig. 15. Variations in r_p with pH on (a) ESNA, (b) HYDRACoRe, and (c) NF 270.

three NF membranes to find the best ANN structure to predict ion rejection. The hidden layer includes seven neurons with tan-sigmoid function. MSE calculations were performed after each iteration to determine the best possible output and performance of the neural network. Since the data were randomly selected, for every set of neurons, the network was run several times.

Ion rejections are obtained as outputs and the input dataset of 65 samples each for the three tested NF membranes were divided into three sets randomly. 70% of the dataset (45 samples) were regarded as train data, 15% of the dataset as validation, and 15% of the data set was regarded for test data (10 samples each). The regression plot for ESNA with seven neurons in the hidden layer is presented in Fig. 16.

Fig. 16 displays the network outputs with respect to targets used for training, validation, and test. The regression plot shows that the R^2 value is 0.996 for training, confirming that the neural network is well trained with 45 samples. The data should fall along the 45° line for a perfect fit where the ANN outputs are equal to the target values provided. R^2 value for test data is also greater than 0.99, confirming that ANN predicted rejection values and experimental values are in close agreement, which signifies the ability of ANN in predicting major ion rejections if flux, pH, and pressure are available.

In this work, seven neurons were selected with the highest accuracy and were compared by changing the transfer function between tansig, logsig, and purlin functions. To optimize the neural network architecture, the computations started with one neuron as the initial guess and the number of neurons was increased after calculating the MSE according

to Eq. (10). Performance of ANN model with some selected network structures is presented in Table 5.

It was confirmed that tansig transfer function works best for predicting ion rejection compared with logsig and purelin transfer functions. The optimal number of seven neurons in the hidden layer was chosen (marked in bold in Table 5) after calculating R^2 and MSE for all four ions tested. A hidden neuron layer of 4, 5, and 6 also provided above 92% for ESNA and NF 270 but a neuron combination of seven provided highest R^2 for all three membranes and least MSE for ion rejection. ANN approach is data-driven and hence is specific for a particular membrane.

5. Conclusions

ANN quantitatively predicted the ion rejection without using any membrane properties such as pore radius, effective membrane thickness, and membrane charge density. ANN is considered as a simple approach for multiple variables compared with membrane process models. An overall agreement was obtained for ANN predictions and experimental results for all three tested NF membranes.

A significant change in rejection was observed even with small pH changes. For divalent ions, a change in rejection was obvious between acidic and alkaline environments. Flux was higher in the basic environment. When flux increased with an increase in pH, the rejection of charged ions tends to decrease. Highest flux was observed for ESNA indicating a larger pore size than for HYDRACoRe and NF 270. A sharp decrease in Mg^{2+} rejection was observed in the

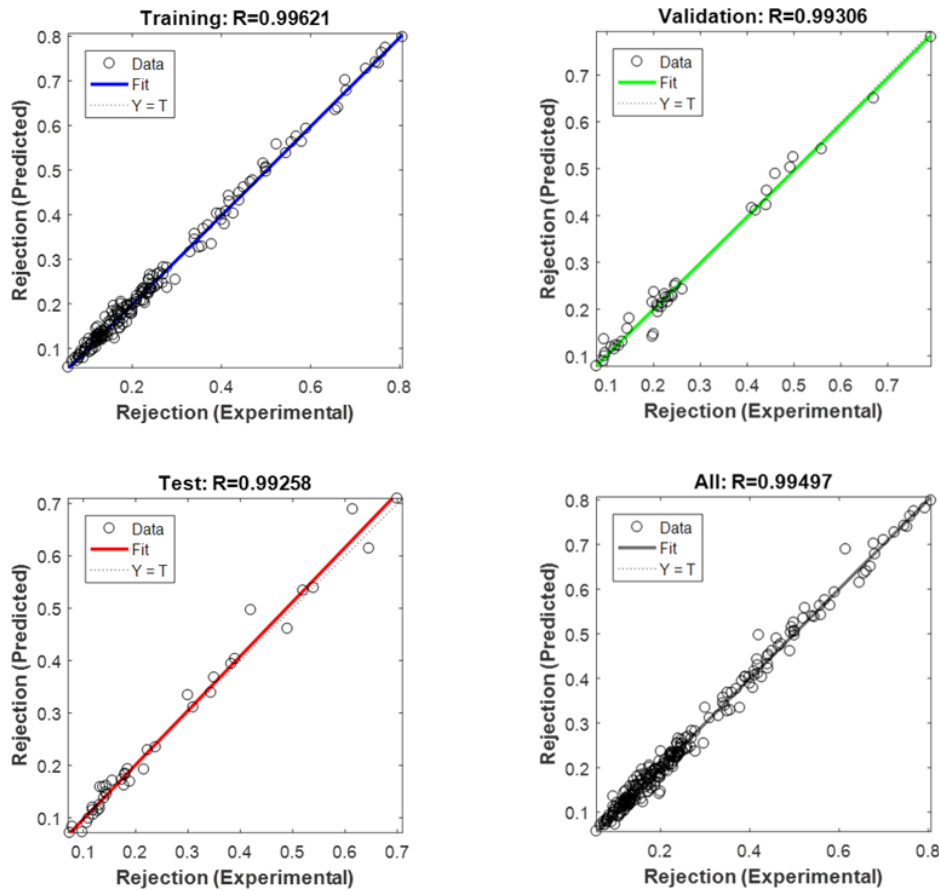


Fig. 16. Regression plot between the experimental and predicted rejection values for ESNA with seven neurons in the hidden layer.

Table 5
Performance of ANN with different neuron and transfer functions

| Membranes | No. of neurons in each layer | R ² | MSE | | | |
|------------------|------------------------------|----------------|-----------------|-----------------|------------------|------------------|
| | | | Cl ⁻ | Na ⁺ | Mg ²⁺ | Ca ²⁺ |
| ESNA | 4 | 0.989 | 0.00014 | 0.00029 | 0.00049 | 0.00096 |
| Filmtec | 4 | 0.97 | 0.00087 | 0.00107 | 0.00086 | 0.01466 |
| HYDRACoRe | 4 | 0.93 | 0.00024 | 0.00035 | 0.00015 | 0.00135 |
| ESNA | 5 | 0.98 | 0.00012 | 0.00026 | 0.00056 | 0.00190 |
| Filmtec | 5 | 0.986 | 0.00057 | 0.00068 | 0.00043 | 0.00709 |
| HYDRACoRe | 5 | 0.94 | 0.00024 | 0.00037 | 0.00011 | 0.00100 |
| ESNA | 7 | 0.995 | 0.00011 | 0.00031 | 0.00030 | 0.00053 |
| Filmtec | 7 | 0.992 | 0.00048 | 0.00052 | 0.00052 | 0.00393 |
| HYDRACoRe | 7 | 0.956 | 0.00022 | 0.00032 | 0.00011 | 0.00013 |
| ESNA | 10 | 0.9925 | 0.00014 | 0.00029 | 0.00049 | 0.00096 |
| Filmtec | 10 | 0.99 | 0.00038 | 0.00036 | 0.00047 | 0.00374 |
| HYDRACoRe | 10 | 0.92 | 0.00029 | 0.00036 | 0.00015 | 0.00162 |

basic environment for ESNA and NF 270. It was confirmed that pore size decreased with a decrease in feed pH using Spiegler–Kedem and SHP models.

Obtained results can be implemented in industrial scale-up for predicting water recovery and ions rejection when PW or other saltwater with varying pH is treated by membranes. These findings are crucial for optimal membrane system

design and for a defined ion rejection as required for smart water production for EOR in carbonate and sandstone reservoirs. pH of PW can be adjusted accordingly for required ion composition in the permeate. For industrial PW applications, the ANN approach to predict NF ion rejection can be used, provided plant operating conditions data for selected feed compositions are available resulting in time and effort savings.

Symbols

| | | |
|----------------|---|--|
| R_{obs} | — | Observed rejection |
| σ | — | Reflection coefficient |
| P_s | — | Solute permeability coefficient, m/s |
| J_v | — | Water flux, L/m ² /h |
| V | — | Permeate volume, L |
| t | — | Filtration time, h |
| A | — | Effective membrane area, m ² |
| S_D, S_F | — | Steric hindrance factors for diffusion and filtration flow |
| D | — | Diffusivity of i -th ion, m ² /s |
| r_s | — | Stokes radius, nm |
| r_p | — | Pore radius, nm |
| $A_k/\Delta x$ | — | Ratio of membrane porosity to membrane thickness |
| C_f | — | Feed concentration, mg/L |
| C_p | — | Permeate concentration, mg/L |
| C_c | — | Retentate concentrations, mg/L |
| t_i | — | i -th target value |
| a_i | — | Predicted value |
| n | — | Number of data |
| R^2 | — | Statistical coefficient of determination |

Acknowledgment

The authors acknowledge the Research Council of Norway and the industry partners, ConocoPhillips Skandinavia AS, Aker BP ASA, Eni Norge AS, Total E&P Norge AS, Equinor ASA, Neptune Energy Norge AS, Lundin Norway AS, Halliburton AS, Schlumberger Norge AS, Wintershall Norge AS, and DEA Norge AS of The National IOR Centre of Norway for support.

References

- [1] Norwegian Oil and Gas industry, Environmental Work by the Oil and Gas Industry- Facts and Development Trends, Published by Norsk olje & gass, 2016.
- [2] T. Austad, Water-based EOR in Carbonates and Sandstone: new Chemical Understanding of the EOR-Potential Using “Smart water”, in J. Sheng, Ed., Enhanced Oil Recovery Field Case Studies; Gulf Professional Publishing, Houston, TX., 2013, pp. 301–335.
- [3] S. Strand, E.J. Høgenesen, T. Austad, Wettability alteration of carbonates- effects of potential determining ions (Ca²⁺ and SO₄²⁻) and temperature, Colloids Surf., A, 275 (2006) 1–10.
- [4] R.R. Nair, E. Protasova, S. Strand, T. Bilstad, Membrane performance analysis for smart water production for enhanced oil recovery in carbonate and sandstone reservoirs, Energy Fuels, 32 (2018) 4988–4995.
- [5] R. Nair, E. Protasova, S. Strand, T. Bilstad, Produced water Treatment with Membranes for Enhanced Oil Recovery in Carbonate and Sandstone Reservoirs, Proc. IOR 2017–19th European Symposium on Improved Oil Recovery, Stavanger, Norway, no. DOI:10.3997/2214-4609.201700296, April 24–27, 2017.
- [6] J.P. Ray, R.F. Engelhardt, Produced Water-Technological/ Environmental Issues and Solutions, Published by Springer, US, 1992.
- [7] M. Reed, S. Johnsen, Produced Water-2-Environmental Issues and Mitigation Technologies, Published by Springer, US, 1996.
- [8] T. Puntervold, T. Austad, Injection of Seawater and Mixtures with Produced Water into North Sea Chalk Formation: Impact on Wettability, Scale Formation, and Rock Mechanics Caused by Fluid-Rock Interaction, Presented at the SPE/EAGE Reservoir Characterization and Simulation Conference, Abu Dhabi, SPE-111237-MS, 2007. Available at: <https://doi.org/10.2118/111237-MS>.
- [9] O. Kedem, A. Katchalsky, Permeability of composite membranes: Part 1. Electric current, volume flow and flow of solutes through membranes, Trans. Faraday Soc., 59 (1963) 1918–1953.
- [10] O. Kedem, A. Katchalsky, Thermodynamical analysis of the permeability of biological membranes to non-electrolytes, Biochim. Biophys. Acta, 27 (1958) 229–246.
- [11] C.K. Diwara, S. Lo, M. Rumeau, M. Pontie, O. Sarr, A phenomenological mass transfer approach in nanofiltration of halide ions for a selective defluorination of brackish drinking water, J. Membr. Sci., 219 (2003) 103–112.
- [12] Z. Murthy, S. Gupta, Estimation of mass transfer coefficient using a combined nonlinear membrane transport and film theory model, Desalination, 109 (1997) 39–49.
- [13] M. Dornier, M. Decloux, G. Trystram, A. Lebert, Dynamic modeling of crossflow microfiltration using neural networks, J. Membr. Sci., 98 (1995) 263–273.
- [14] H. Al-Zoubi, N. Hilal, N. Darwish, A. Mohammad, Rejection and modeling of sulphate and potassium salts by nanofiltration membranes: neural network and Spiegler-Kedem model, Desalination, 206 (2007) 42–60.
- [15] W. Bowen, M. Jones, H. Yousef, Dynamic ultrafiltration of proteins - a neural network approach, J. Membr. Sci., 146 (1998) 225–235.
- [16] S. Bandini, J. Drei, D. Vezzani, The role of pH and concentration on the ion rejection in polyamide nanofiltration membranes, J. Membr. Sci., 264 (2005) 65–74.
- [17] F. Donnan, Theory of membrane equilibria and membrane potentials in the presence of non-dialysing electrolytes. A contribution to physical.chemical physiology, J. Membr. Sci., 100 (1995) 45–55.
- [18] W.R. Bowen, A.W. Mohammad, N. Hilal, Characterisation of nanofiltration membranes for predictive purposes – use of salts, uncharged solutes, atomic force microscopy, J. Membr. Sci., 126 (1997) 91–105.
- [19] J. Schaep, C. Vandecasteele, W. Mohammad, R. Bowen, Modeling the retention of ionic components for different nanofiltration membranes, Sep. Purif. Technol., 22–23 (2001) 169–179.
- [20] K. Spiegler, O. Kedem, Thermodynamics of hyperfiltration (reverse osmosis): criteria for efficient membranes, Desalination, 1 (1966) 311–326.
- [21] S.-I. Nakao, S. Kimura, Models of membrane transport phenomena and their applications for ultrafiltration data, J. Chem. Eng. Japan, 15 (1982) 200–205.
- [22] X. Wang, T. Tsuru, S.-i. Nakao, S. Kimura, The electrostatic and steric-hindrance model for the transport of charged solutes through nanofiltration membranes, J. Membr. Sci., 135 (1997) 19–32.
- [23] X.-L. Wang, T. Tsuru, M. Togoh, S.-I. Nakao, S. Kimura, Evaluation of pore structure and electrical properties of nanofiltration membranes, J. Chem. Eng. Japan, 28 (1995) 186–192.
- [24] R. Bowen, W. Mohammad, Diafiltration by nanofiltration: prediction and optimization, AIChE J., 44 (1998) 1799–1812.
- [25] W. Bowen, J.S. Welfoot, P. Williams, Linearized transport model for nanofiltration: development and Assessment, AIChE J., 44 (2002) 760–773.
- [26] M.H. Beale, M.T. Hagen, H. Demuth, Neural Networks Toolbox (TM)– Users guide, The MathWorks, Inc., 2018. Available at: <https://usermanual.wiki/Document/Neural20Network20User20Guide.1353260851.pdf>
- [27] M. Cheryan, Ultrafiltration and Microfiltration Handbook, CRC Press, USA, 1998.
- [28] M. Manttari, A. Pihlajamaki, M. Nystrom, Effect of pH on hydrophilicity and charge and their effect on the filtration efficiency of NF membranes at different pH, J. Membr. Sci., 280 (2006) 311–320.
- [29] B. Tansel, Significance of thermodynamic and physical characteristics on permeation of ions during membrane separation : hydrated radius, hydration free energy and viscous effects, Sep. Purif. Technol., 86 (2012) 119–126.